

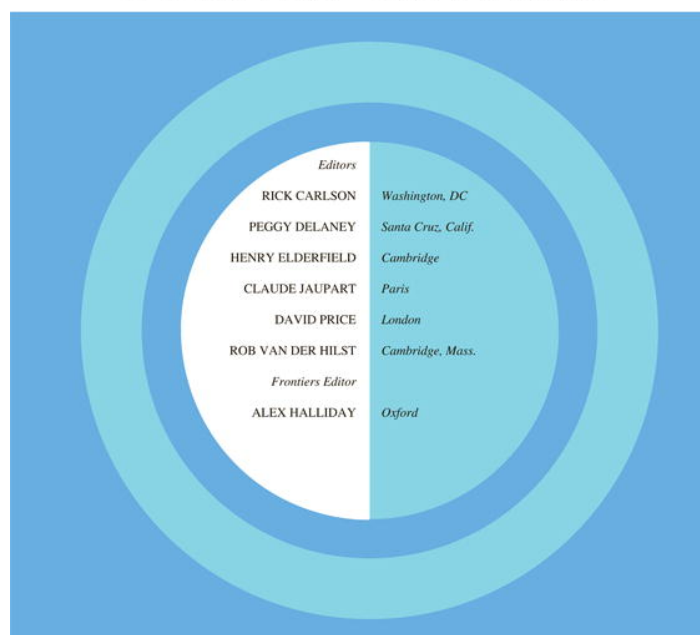


Volume 248, Issues 3–4

30 August 2006

ISSN 0012-821X

EARTH AND PLANETARY SCIENCE LETTERS



<http://www.elsevier.com/locate/epsl>

This article was originally published in a journal published by Elsevier, and the attached copy is provided by Elsevier for the author's benefit and for the benefit of the author's institution, for non-commercial research and educational use including without limitation use in instruction at your institution, sending it to specific colleagues that you know, and providing a copy to your institution's administrator.

All other uses, reproduction and distribution, including without limitation commercial reprints, selling or licensing copies or access, or posting on open internet sites, your personal or institution's website or repository, are prohibited. For exceptions, permission may be sought for such use through Elsevier's permissions site at:

<http://www.elsevier.com/locate/permissionusematerial>



ELSEVIER

Available online at www.sciencedirect.com

ScienceDirect

Earth and Planetary Science Letters 248 (2006) 685–699

EPSL

www.elsevier.com/locate/epsl

Plume fluxes from seismic tomography

Guust Nolet^{a,*}, Shun-Ichiro Karato^b, Raffaella Montelli^{a,1}

^a Department of Geosciences, Princeton University, Princeton, NJ 08544, USA

^b Department of Geology and Geophysics, Yale University, New Haven, CT 06520, USA

Received 30 March 2006; received in revised form 2 June 2006; accepted 8 June 2006

Available online 21 July 2006

Editor: C.P. Jaupart

Abstract

We use mantle plume images from finite frequency tomography and the Stokes equation to obtain a quantitative estimate of the heat and volume flux across several well resolved plume sections in mid-mantle. Although not a perfect barrier, widening of plumes just below 670 km depth indicates that the phase transition from ringwoodite to perovskite plus magnesowüstite and possibly iron enrichment of the lower mantle resists plume passage into the upper mantle. Estimated heat- and volume flux for individual plumes at mid-mantle depths is greater than predicted by surface observations of buoyancy flux, even for very high viscosity. Although uncertainties are large, the high flux observed in plumes at mid-mantle depth is compatible with the view that plumes are responsible for all upward advective heat transport in the lower mantle that eventually breaks through into the upper mantle.

© 2006 Elsevier B.V. All rights reserved.

Keywords: Mantle heat flux; Plumes; Lower mantle heterogeneity

1. Introduction

The Earth radiates about 44 TW (teraWatt or 10^{12} J/s) into space. Part of this energy is generated by radioactive decay of long-lived isotopes, mostly U, Th and K, part is due to secular cooling of the planet. The ratio between the two, the Urey number, is subject of intense debate [1,2]. But whatever the value of the Urey number, a substantial fraction of the heat flux must come from the lower mantle or core.

The lack of topography associated with buoyant upwellings generated at a possible thermal boundary layer precludes that heat moves from lower to upper

mantle by conduction [3]. Both slabs and plumes are obvious candidates for heat transport by advection. In this paper we investigate if new tomographic results support the widely accepted view that only a small fraction (3 TW) of heat transport from lower to upper mantle is effected through plumes located beneath known, strong hotspots [3–5]. This view is based on the estimated values of the buoyancy flux for a number of plumes. The buoyancy flux B relates to the heat flux Q_c^{surf} near the surface through the thermal expansivity α and the heat capacity c_P : $B = \alpha c_P^{-1} Q_c^{\text{surf}}$. For reasonable values of α and c_P near the surface of the Earth, this translates to a surface heat flux of

$$Q_c^{\text{surf}} = 4.2 \times 10^7 B \quad (1)$$

if B is in kg/s and Q_c in Watt. Sleep [4] gives a total buoyancy flux of 5.49×10^4 kg/s which translates to

* Corresponding author.

E-mail address: nolet@princeton.edu (G. Nolet).

¹ Present address: ExxonMobil Upstream Research Company, Houston TX 77252-2189, USA.

2.3 TW, or only 5% of the total heat flux of the Earth. Adding the contribution of flood basalts averaged over time this could be raised to 3.3 TW [6].

Seismic evidence for the existence of plumes in the lower mantle was until recently indirect (see Nataf [7] for a review). Broad lower mantle upwellings or ‘superplumes’ appeared in global tomographic studies in the past decade (see Romanowicz [8] for references). Plume-like features in the lower mantle were first imaged seismologically under Iceland [9], Central Europe [10], Africa [11], and a number of hotspots in the Pacific and Indo–Atlantic region [12,13]. The introduction of finite frequency tomography [14] greatly improved the imaging by correcting for ‘wavefront healing’, and the first study using this new technique resulted in tomographic images of the mantle with some twenty plumes that reach clearly below the 670 km discontinuity and that were shown to have diameters of 500 km or more [15]. Recently, Montelli et al. [16] improved this model (PRI-P05) and presented confirming evidence for lower mantle plumes from independent data (long-period S waves). The large width of the plumes suggests that they play a much more substantial role in heat transport than is implied by the 3 TW estimate. Simply put: plumes are difficult to resolve, if they were not big we wouldn’t be able to see them, and assuming they have the heat capacity that befits them, they are important in the Earth’s heat budget. Estimates from topographic swells are so far the only direct quantitative observations we have for plume fluxes. The first direct tomographic images of plumes seem to contradict these estimates at least in a qualitative sense. This paper is a first attempt to make this statement a little more quantitative. Though we realize that the uncertainties are very large, it is important to investigate if at least an agreement within an order of magnitude can be obtained for plume fluxes obtained from tomography and from surface observations.

The progress in plume imaging is such that we can make reasonably accurate estimates of the plume temperature anomaly for several well-resolved plume sections. This enables us to estimate the heat capacity of the plume. However, to calculate the *flux*, we also need to know the rise velocity v_z of the plume which makes additional demands on resolution quality and plume geometry. In this paper we use a simple model based on Poiseuille flow to derive approximate plume fluxes from the tomographic images. We assume a balance between frictional and buoyancy force at well-resolved cross-sections of several plumes. This assumption implies that the flow is predominantly vertical and that we are far away from the top or bottom of the plume where boundary forces operate. In fact, we shall see that the computations give nonphysical results at shallow levels, and we use this as a diagnostic that

the assumption of vertical flow breaks down near the top of the plume. Surprisingly, the ‘top’ boundary is not necessarily the Earth’s surface. In inspecting the plume images in model PRI-P05, it is remarkable how many plumes change character at the 670 km discontinuity. The role of this phase transition as a possible boundary for plumes is discussed in the next section.

2. The role of the 670 km discontinuity

Fig. 1 gives a good example of a plume meeting resistance upon entering the upper mantle. The large anomaly near the core–mantle boundary is linked to the African superplume. Temperatures are computed assuming a perovskite–magnesiowüstite composition, which may not be correct in the deepest part of the mantle, as exemplified in the blow-up of cold as well as hot anomalies. Canary rises up from the superplume. The Cape Verde plume further south is less well resolved and the merging of the plumes at mid-mantle depth may very well be a resolution artifact, as shown in the lower half of Fig. 1. At 670 the plume changes abruptly in character, and is very weak in the upper mantle. With broadband stations (TBT and SACV) on top of both plumes and several ISC-reporting stations on Cape Verde islands, the change in character cannot easily be attributed to lack of resolution, an observation that is confirmed by the resolution tests in [15]. Note also that even the upper mantle signal beneath the Azores shows up as an anomaly despite a relative lack of resolution.

Fig. 2 shows four more examples of plumes that broaden or deflect significantly when approaching the 670 km discontinuity. Resolution calculations for these plumes similar to those shown in Fig. 1 show that the spreading below the 670 is not a resolution artifact. In the case of Easter and Tahiti, the plume has broken through and reaches the surface.

The apparent hesitancy of several plumes to penetrate the phase transition resembles that of some slabs that reside in the transition zone before breaking through and sink into the lower mantle [17]. The spreading of plume material in the mesosphere which we observe here was hypothesized by Allègre [18] to explain the geochemical characteristics of basalts. However, the situation is not universal. In fact, several plumes seem to experience little resistance, as shown in Fig. 3, a situation also reminiscent of that observed for slabs. Others such as Bouvet, Hainan, Hokkaido or Juan Fernandez appear as a blob just below 670 km, whereas Afar, Kerguelen, Bowie, Galapagos and Iceland seem to be stalling blobs that have broken through into the upper mantle (images not shown, but see [16]).

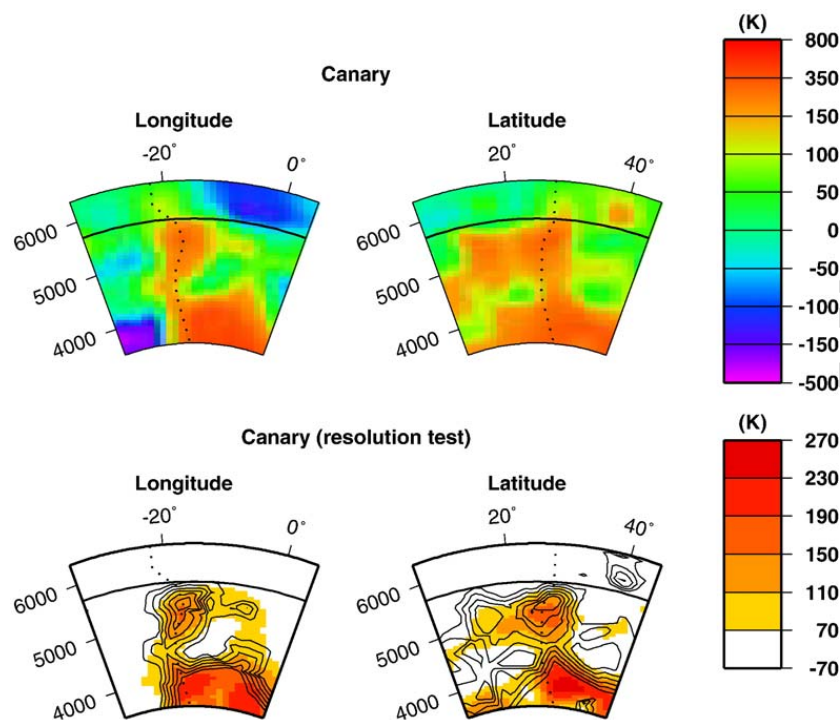


Fig. 1. Two vertical cross-sections through the complex Canary/Cape Verde plume system. The velocity anomalies of the original model PRI-P05 have been translated into a temperature anomaly assuming a perovskite–magnesiowüstite mineralogy (Fig. 4). The vertical axis is the Earth radius and ranges between 3480 km at the core–mantle boundary and 6371 km at the surface. The 670 km discontinuity is indicated by a thick line at $R=5700$ km. The orientations of the planes are west–east (left) and south–north (right), but the cross-sectional planes are slightly warped to follow the maximum temperature anomaly. The dotted line in the left image gives the longitude of the right image at the corresponding depth, and vice versa for the latitude of the left section. The bottom figure gives the result of the resolution test tailored to the original plume image. The contour lines denote a synthetic plume, for which artificial delay times have been computed. The colour scale gives the output of the inversion. Note that the colour scale for the resolution tests is discrete, and changes at the contour levels (in steps of 40 K starting at 70 K). The resolution in the bottom right image strongly suggests that Cape Verde and Canary in reality are separate plumes (at 15° N and 28° N, respectively) but the tomographic image smears them into one between radius 4900 and 5600 km (depths 800–1500 km).

Theoretically, the negative Clapeyron slope of the phase transition at 670 km depth is expected to resist downward penetration of cold material or upward penetration of hot material. The situation is not completely symmetric, since the phase relations may be different at cold and hot temperatures. The maximum temperature anomaly at the center of plumes is smaller than that in slabs, and the higher viscosity of slabs provides a stress guide that can aid penetration, which may more than offset the fact that plumes should have little resistance to rise once its perovskite is transformed to wadsleyite. But even if it is easier for plumes than for slabs to break through, the requirement that mass needs to be conserved would imply that either all slab material entering the lower mantle is replaced by an equal mass flux upward or that the 670 km discontinuity is temporarily displaced to a greater depth (depending on the kinematics of the phase transition), thus reducing the buoyancy of plumes at 670 km depth and inducing a resistance after all. Some numerical experiments indeed show plumes stalling at 670 km [19,20], especially for negative Clapeyron slopes of -3 MPa/K or more.

3. Modeling plume flux

The mantle plume images obtained by Montelli et al. [16], using finite-frequency seismic tomography, offer an opportunity to study deep mantle plumes quantitatively. We stress that this is a first attempt of this kind; the results of this paper will be in need of refinement and are to be viewed as first-order results only. As we shall discuss, the range of acceptable viscosities alone already results in an uncertainty by a factor of at least three — perhaps even a full order of magnitude if one is pessimistic, dwarfing the possible errors made by the simplifications in the physics. But even while fully acknowledging the large uncertainties, some interesting conclusions can be reached.

The P wave model is an update of the model published by [15], using improved and adjusted crustal corrections. The new model, which we use in this study, agrees well with a S velocity model from the inversion of long period S and SS waves. Unfortunately, the lack of high frequency S waves does not allow us to constrain plume width well enough to try a similar flux estimation

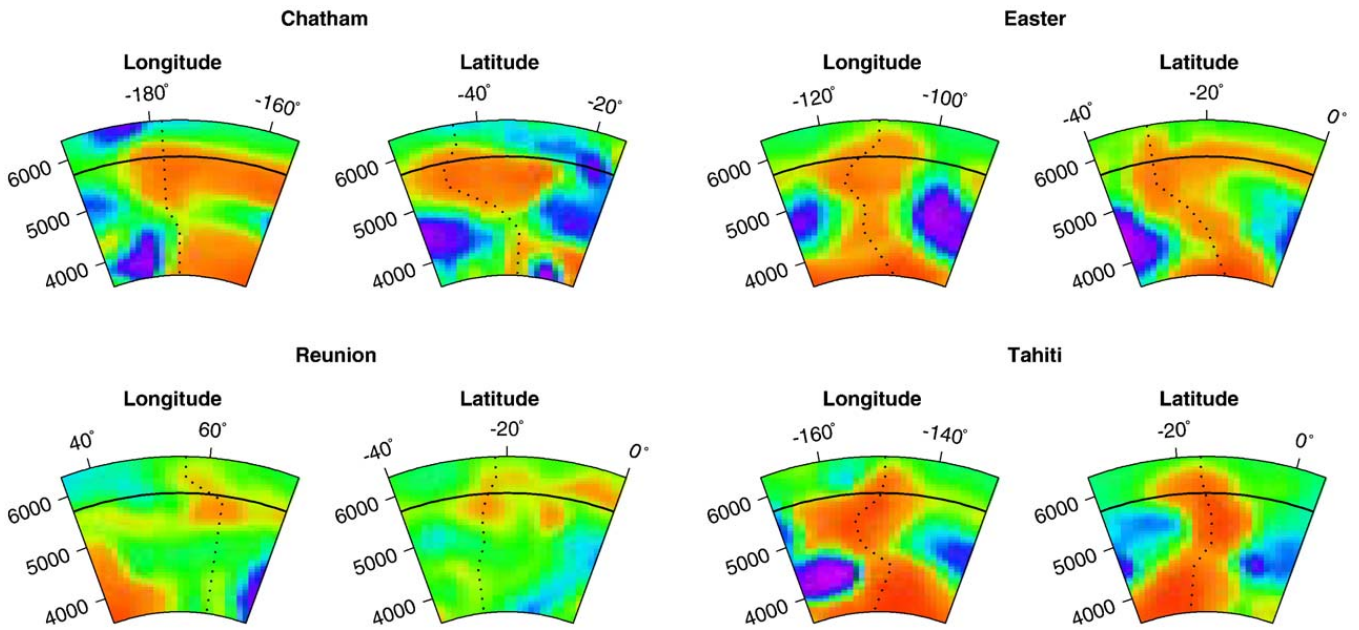


Fig. 2. Four examples of plumes that widen or even get stuck below the 670 km discontinuity. Resolution tests similar to the one shown in Fig. 1 show that the broadening or deflection at the top of the mantle is resolved for each of these plumes. The temperature scale is the same as in Fig. 1 (top).

from the S anomalies. The Princeton group has embarked on an ambitious observational program to measure arrival times and amplitudes of seismic waves in a range of frequency bands, which fully exploits the possibilities of finite-frequency theory [21] and we hope to be able to compare P and S flux estimates in the future.

Montelli et al. [16] estimate the changes in the relative compressional seismic velocity ($\Delta V_P/V_P = \Delta \ln V_P$).

Using theoretical values of the temperature derivative $\partial \ln V_P / \partial T$ (Fig. 4) we convert these to anomalies ΔT .

Thus, because they give us an indirect measure of the temperature anomaly inside the plume, the tomographic images allow us to break away from purely theoretical models of mantle plumes [22] that solve for both temperature and rise velocity by specifying boundary conditions at top and bottom of the mantle. Ideally our method

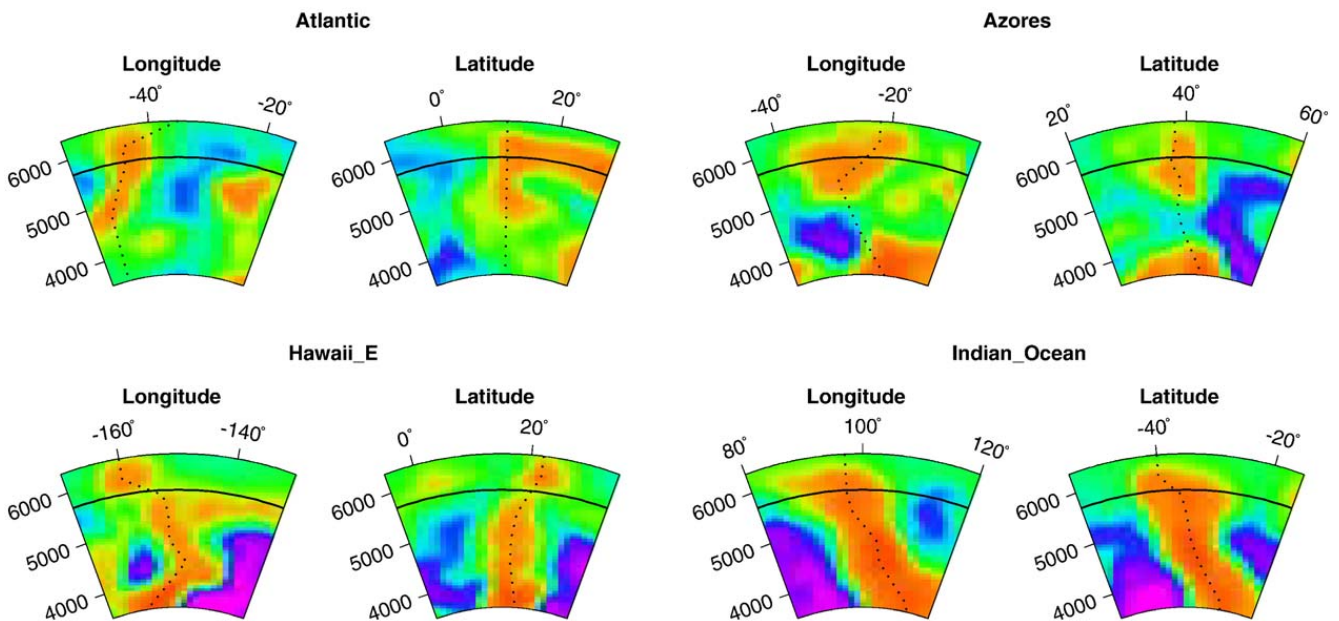


Fig. 3. As Fig. 2, now showing plumes that meet little resistance at 670 km or that may just have 'broken through'. The temperature scale is the same as in Fig. 1 (top).

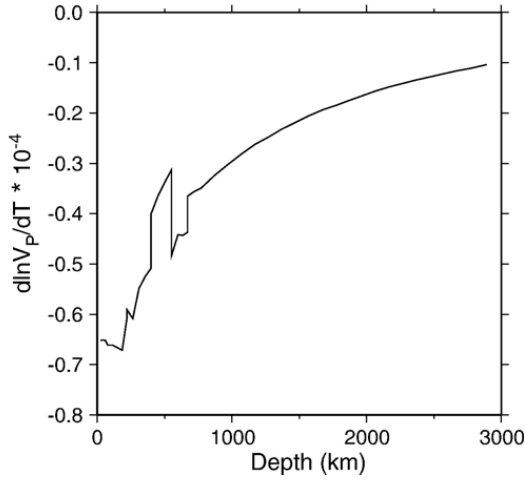


Fig. 4. Anharmonic temperature derivative of $d \ln V_P / dT = V_P^{-1} dV_P / dT$ (in units of K^{-1} times 10^{-4}) used to convert V_P anomalies into ΔT , see Eq. (5).

works as follows: given the coefficient of thermal expansion, we compute the density difference between the plume and its surroundings. Chemical contributions to this difference can easily be added. Then, if we know the viscosity, we can solve the dynamic equations and get an idea of the present-day flow in the Earth's mantle. In practice, there are several hurdles to overcome. The lower-mantle viscosity is one of the least well constrained parameters; iron enrichment in the plume is a realistic possibility, but to what degree is virtually unknown; and last but not least the tomographic resolution is only locally good enough to resolve plumes adequately.

Faced with these difficulties, we compromise between a theoretical solution and a full-fledged fluid dynamic interpretation for the whole global sphere. Instead, we see the plume as a simple conduit and we assume that at any one depth a dynamic equilibrium exists between the buoyancy and the friction, thus reducing the problem to a local force balance in two dimensions. Some support for this approximation was provided by U. Hansen (pers. comm. 2004) who showed that this approximation is justified with errors locally as low as 10% in the force contributions in 3D numerical calculations for both temperature-dependent and constant viscosity, except near the upper and lower boundaries of the plume. We find the local rise velocity of the plume solving (Stokes' equation):

$$\nabla \cdot [\eta(T) \nabla v_z] \approx \eta(T) \nabla^2 v_z = -\alpha \rho g \Delta T + g \Delta \rho_c \quad (2)$$

where $\nabla = (\partial_x, \partial_y)$ is the horizontal gradient, η is the dynamic viscosity, v_z is the plume rise velocity, g the acceleration of gravity and $\Delta \rho_c$ the density change caused by a change in composition of the plume with

respect to the surrounding mantle. The parameters $\eta(T)$, v_z and ΔT depend on the cross-sectional coordinates x and y . The volume and heat fluxes through the cross-section S are then found by integration:

$$Q_V^{\text{plume}} = \int_S \rho v_z(x, y) dx dy \quad (3)$$

$$Q_c^{\text{plume}} = \int_S \rho c_P v_z(x, y) \Delta T(x, y) dx dy \quad (4)$$

To speed up the calculations, we neglect the term $\nabla \eta \cdot \nabla v_z$ in the Stokes Eq. (2), thereby reducing it to an elliptical equation that can stably and efficiently be solved by relaxation methods. Note that we do not neglect the temperature dependence of η , and numerical checks using a temperature dependent viscosity with activation energies ranging from 400 to 500 kJ/mol show that the error induced by this approximation in the total heat flux is only of the order of a few percent, not surprisingly because both $\nabla \eta$ and ∇v_z are zero at the plume center where both ∇v_z^2 and the flux $v_z \Delta T$ itself are the largest. In any case, the small error introduced by the approximation is far less than the spread possible in the force terms of Eq. (2) caused by the uncertainty in the model parameters.

We assume that $v_z = 0$ outside of the region where the net buoyancy force is positive, or where $\Delta T < \Delta T_{\text{lim}}$, whichever is reached earlier. Following [23] and [24], the temperature boundary condition has been implemented to avoid that more 'normal' mantle flow is interpreted as plume flux. We neglect any mass transfer in or from the halo beyond this limit [25]. We test the influence of the boundary condition by repeating the computations for $\Delta T_{\text{lim}} = 70, 110$ and 150 K. Because of the uncertainty in the tomographic images, lowering ΔT_{lim} to much lower values is not possible. However, as we shall see, the flux is dominated by the flux at the center at the plume where the temperature is highest and the viscosity appreciably reduced, which limits the dependence of the flux estimate on the choice of ΔT_{lim} .

We start the calculations by scanning the tomographic model for negative velocity anomalies. An algorithm searches for the connected region where ΔT is in excess of ΔT_{lim} at a series of depths between 1100 and 2000 km in steps of 100 km and solves Eq. (2) at each of these levels. In earlier reports on this work we concentrated on plume cross-sections near the top of the lower mantle that are particularly well resolved [26]. As argued in the previous section, the 670 discontinuity may present a barrier to upward flow that is non-negligible, thereby making our

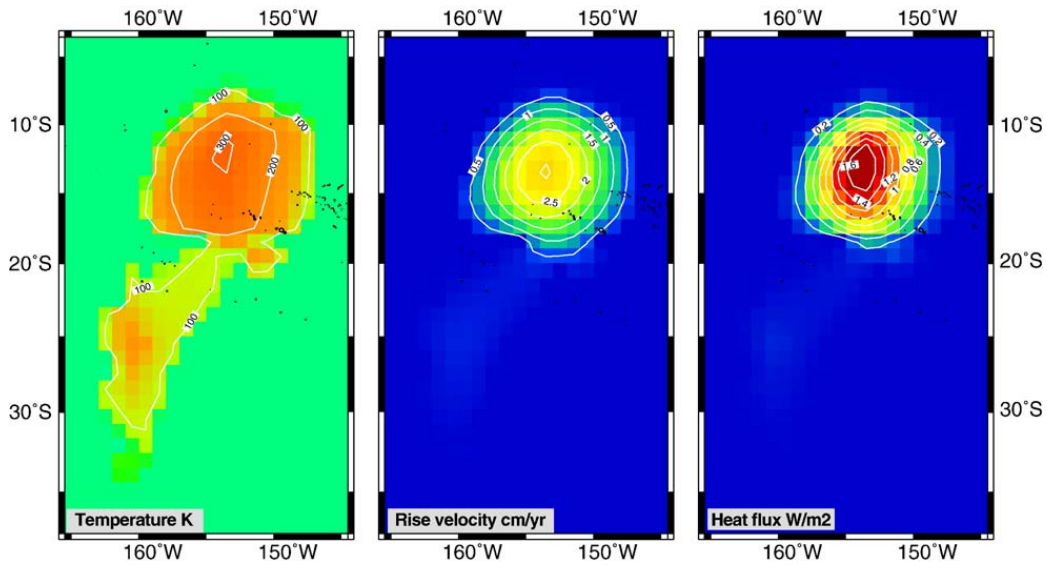


Fig. 5. Illustration, from left to right, of the most important steps in the heat flux analysis, for the Tahiti plume at a depth of 1600 km. (left) The P -velocity anomaly as determined by a finite-frequency inversion of delay times is converted to a temperature anomaly $\Delta T = \Delta \ln V_P / (\partial \ln V_P / \partial T)$. Temperature contours in Kelvin. (center) Solving Eq. (2) yields the rise velocity of plume. Velocity contours in cm/yr. (right) Finally, we compute the heat flux $c_p \rho v_z \Delta T$. Contours in W/m^2 .

simple force-balance approach questionable near the top of the lower mantle. As a result, we shall restrict our attention to the mid-mantle plumes that are well resolved and far below the 670 km discontinuity. Cross-sections in the lowermost part of the mantle are not well resolved. Moreover, we notice that below 2300 km depth both negative and positive temperature anomalies become more pronounced. This could mean that either the adopted $d \ln V_P / dT$ is not correct or that the background model is significantly too slow, leading to an overestimation of the magnitude of cold—but underestimation of the magnitude of hot anomalies. In either case, we judged it wise to refrain from interpretations below 2000 km, and restricted attention to plumes that have sufficient resolution. Blobs that show no vertical continuity are discarded. However, several anomalies with clear vertical continuity were added to our list of plumes, e.g. the columnar anomalies observed under the Atlantic Ridge and Indian Ocean, as well as starting plumes only visible in the lowermost mantle, such as the one South of Java.

Fig. 5 illustrates our approach for a cross-section through the plume that is visible beneath Tahiti. For this particular modeling we used a local background viscosity of 1.2×10^{23} Pa s as in Fig. 6, and no iron enrichment. The rise velocity is 3.2 cm/yr, the total volume flux $12 \text{ km}^3/\text{yr}$, the total heat flux 0.53 TW. Resolution analysis (see next section) shows that ΔV_P is damped in the image, causing Q_c to be underestimated by 34%, such that an unbiased estimate would be raised to 0.80 TW. This exceeds the flux estimated from the buoyancy flux of 3.3 Mg/s [4] by a factor of six. If the lower mantle flux measured here feeds

the Tahiti, MacDonald and the Marquesas Islands swells, the total buoyancy flux is 9.9 Mg/s which corresponds to 0.42 TW, about half the flux from tomography (Davies [5] gives a total flux of 14.3 Mg/s or 0.60 TW). This brings lower and upper mantle fluxes closer, and is compatible with a model in which hot material spreads locally below 670 km to spawn separate plumes in the upper mantle.

The diameter of the main conduit of the plume as measured by the level where ΔT is 1/2 of its maximum, is of the order of 1000 km. The weaker temperature anomaly protruding towards the southwest is too narrow and viscous to generate much of a flux and the plume itself is quite cylindrical. Defined by the half value of v_z , the plume

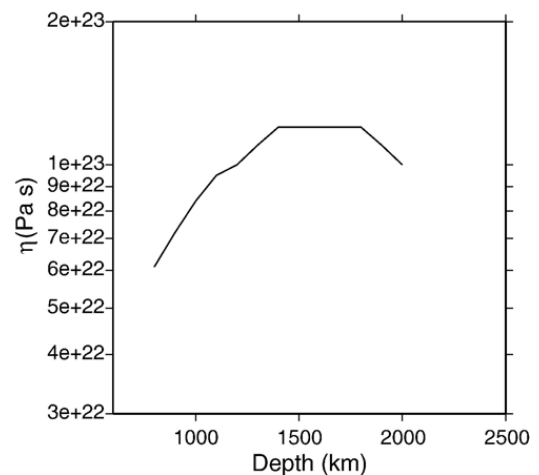


Fig. 6. The dynamic viscosity used in the calculations. The viscosity is fixed at 6×10^{22} Pa s at a depth of 800 km, then follows an Arrhenius law. See text for discussion of uncertainties.

narrows down to 800 km. The image of Q_c^{plume} , which involves the product $v_z \Delta T$ has a width of about 700 km.

4. Resolution bias

The accuracy of our estimates is a strong function of the resolving power of the seismic tomography. Seismic images present a somewhat smoothed or blurred version of the true Earth. Two effects of different sign compete in building up a bias in the inferred flux. Whereas the widening of the image will *increase* the estimate of the flow (much as in Poiseuille's law of flow through a wider pipe), the spreading of the anomaly in the image dampens ΔT , which reduces the buoyancy force as well as the effective plume radius where $\Delta T = \Delta T_{\text{lim}}$, and thus *reduces* the calculated volume flux. The dampening of anomalies has an even greater effect on the heat flux since it not only reduces the volume flux but also the total heat content of the plume.

To estimate the net statistical bias induced by these effects, we follow standard practice, and repeat all of our calculations for a 'synthetic' model for which we know the answers. The synthetic model has plume-like features modeled after the real tomographic images, and is used to create synthetic data, which upon inversion give an output model close to the actual tomographic image. We test the

influence of the choice of ΔT_{lim} by repeating the computations for various ΔT_{lim} . Examples for eight plume cross-sections are given in Fig. 7. A visual comparison of such resolution tests is used to judge the effects of regularizations. Just comparing visually is not sufficient, however, because even small changes in the radius of the plume may have large effects on computed fluxes. We therefore compute temperatures as well as heat- and volume fluxes for both input- and output model, compare, and reject if the difference in any one of them is too large.

The maximum temperature anomaly ΔT_{max} , and the fluxes Q_c^{plume} and Q_V^{plume} differ in their sensitivity to tomographic errors (see Eqs. (3) and (4)), and by requiring each of these to be within reasonable limits, we reduce the possibility that a good agreement between input and output fluxes is obtained by pure chance. Fig. 8 shows the bias factors. Of 165 visually well-resolved cross-sections, 66 had a bias factor for Q_c between 0.5 and 2 (75 for Q_V). At first sight a bias of the order of 2 may seem like an unsurmountable handicap but one must realize that it is very small with respect to the uncertainty of a factor of 3–10 in viscosity, which directly translates into the same factor of uncertainty in computed flux predictions.

We left the African Superplume out of consideration even though it is very well resolved, because its width is too large to warrant the simplifications we made, and

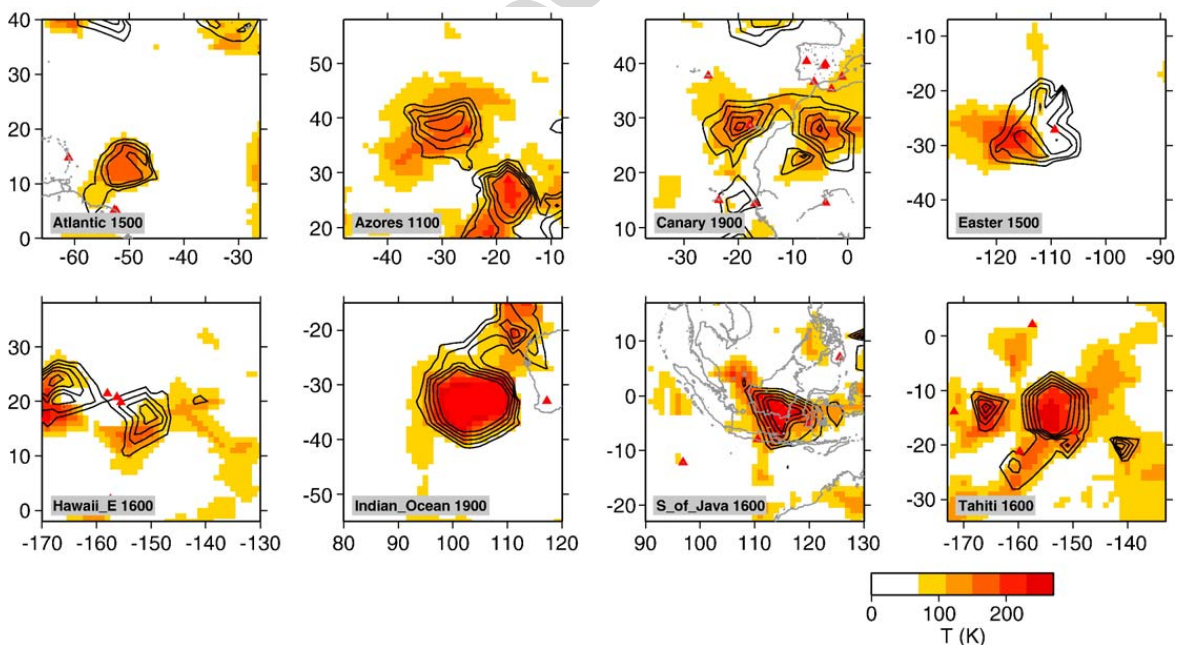


Fig. 7. This figure illustrates resolution tests for eight different plume cross-sections. A synthetic model is given by contour lines. A tomographic solution is obtained by inverting data generated by the synthetic model, and is given by the colour scale. To neutralize the changes of $\partial V_p / \partial T$ with depth, we plot temperature rather than ΔV_p anomalies. For this resolution analysis, we simply used the anharmonic derivatives to convert to temperature. The plumes and the cross-section depths are indicated in the lower left corner of each map. Contour lines start at $\Delta T = 70$ K and increase in steps of 40 K, as does the colour scale. These synthetic plumes closely resemble the plumes visible in model PRI-P05. The mismatches between contour lines (input) and colour scale anomalies (output) are an indication of lack of resolution.

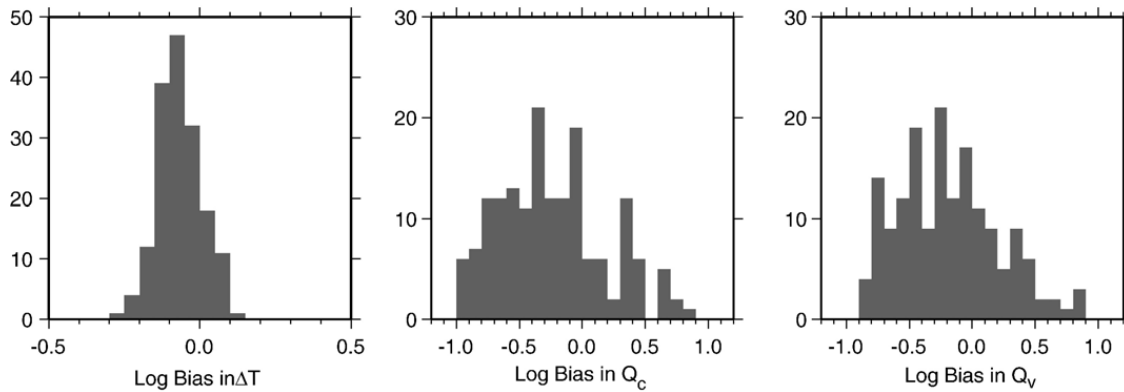


Fig. 8. Histograms for the $^{10}\log$ of the bias factors in 165 plume cross-sections in mid-mantle (depths 1000–2000 km).

chemical heterogeneity may almost certainly play an important role in the dynamics of this ‘plume’. With a ΔT_{\max} of 439 K, the estimated heat flux Q_c is 25.4 TW and the volume flux Q_v is 477 km³/yr. This volume flux would be more than double that of subducted oceanic lithosphere, another indication that the African Superplume is not an ordinary, rising plume.

Fig. 9 shows the dependence of the flux calculations (as a function of depth) on the assumed ΔT_{lim} . With few exceptions, the temperature gradient is large enough to preclude a very strong dependence of the estimated flux on this boundary condition. The figure also shows that the heat flux increases dramatically as the plume nears the 670 km discontinuity. The plume temperature anomalies remain near 200 K, so this increase is mostly a consequence of the widening of the plumes. This implies a

breakdown of our assumption that flow is predominantly vertical and led us to reject any flux estimates shallower than 1100 km. It supports the observation in Section 2, though, that plumes meet resistance at the boundary between lower and upper mantle.

5. Parameter uncertainties

Added to the estimation errors from lack of resolution is the fact that most parameters used are only approximately known. In this section we discuss our parameter choices and their uncertainties.

The temperature derivative $\partial V_p / \partial T$ of the likely lower mantle composition of perovskite and magnesio-wüstite is only approximately known [27–31]. Our preferred curve for the anharmonic derivative is given in

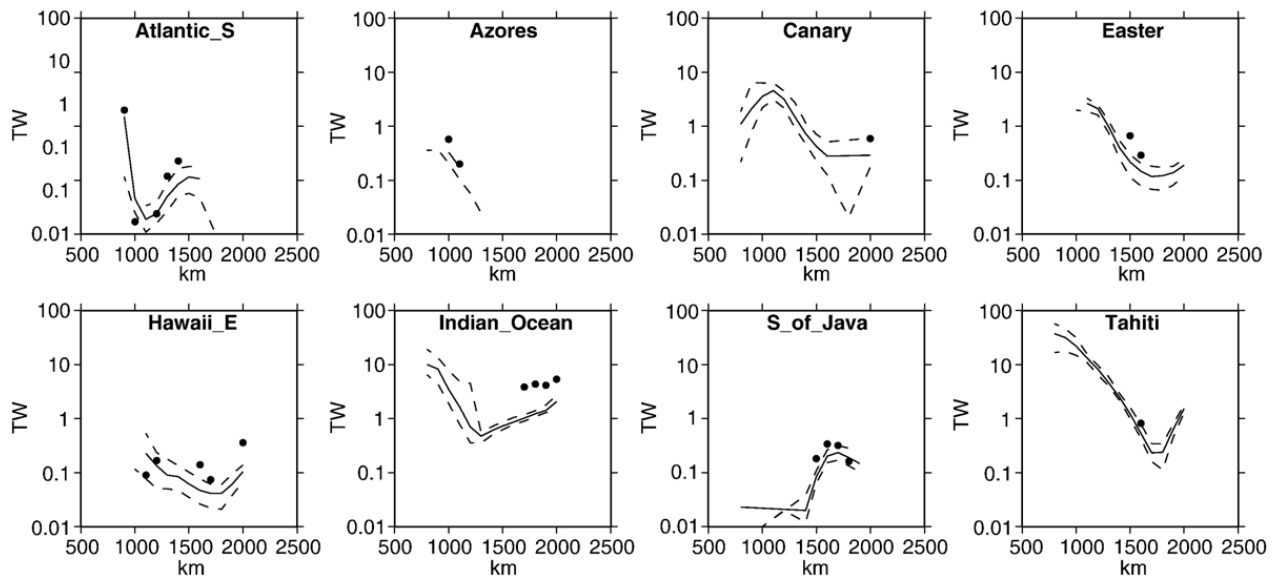


Fig. 9. Plume flux calculations for selected plumes. Solid lines show flux estimates for the plume boundary fixed at $\Delta T_{\text{lim}} = 110$ K, dashed lines show alternative calculations for 70 and 150 K, giving higher and lower flux, respectively. Dots indicate well resolved estimates for $\Delta T = 110$ K after correction for resolution bias. The rapid growth towards the upper mantle boundary, visible in all but the Java plume, is due to widening of the plumes and interpreted as a breakdown of local force balance due to resisting forces from the phase transition at 670 km depth.

Fig. 4. We correct the anharmonic partial derivative $\partial V_P/\partial T$ for anelastic effects using [32]:

$$\left(\frac{\partial \ln V_P}{\partial T}\right) = \left(\frac{\partial \ln V_P}{\partial T}\right)_{\text{anh}} - \frac{\pi p}{2} \cot\left(\frac{\pi p}{2}\right) Q_P^{-1}(\omega, T) \left(\frac{\beta T_m}{\pi T_2}\right) \quad (5)$$

using a quality factor $Q_P(\omega, T)$ with a frequency dependence ω^p (we use $p=0.3$) and a temperature dependence:

$$Q_P(\omega, T) = Q_P(\omega, T_0) \exp(p\beta T_m(1/T - 1/T_0)) \quad (6)$$

Note that this makes the relationship between V_P and ΔT nonlinear, and we iterate until convergence is obtained. For $Q_P(\omega, T_0)$ we adopted the PREM values (at 1 Hz). β scales the activation enthalpy to the melting temperature T_m . The dimensionless constant $\beta = H^*/RT_m$ represents the dependence of activation enthalpy H^* as a function of melting temperature T_m and pressure with R the gas constant (8.3 J/mol/K). β was set to 12, which corresponds to activation enthalpies of 400–500 kJ/mol for the range of T_m , but values between 10 and 15 are generally considered acceptable. For a given ΔV_P Eq. (5) is solved iteratively until it converges to the same $T = T_0 + (\partial \ln V_P/\partial T)^{-1} \Delta V_P$. We consider the values of $\partial V_P/\partial T$ to be uncertain to at least 20%.

Estimates for the thermal expansion are available from theoretical calculations using the quasi-harmonic approximation [27], from Raman spectroscopy [33] and synchrotron X-ray diffraction [34]. Using these results, we fixed the average α_0 at 1471 km depth to $1.4 \times 10^{-5} \text{ K}^{-1}$ and varied the average thermal expansion with depth as

$$\frac{\alpha}{\alpha_0} = \left(\frac{\rho_0}{\rho}\right)^{\delta_T} \quad (7)$$

where $\delta_T=4$ is the Anderson–Grüneisen parameter. The heat capacity C_p is less uncertain. Because the temperature of the rock is well above the Debye temperature, the Dulong–Petit law predicts a constant value, in our case 1250 J/kg/K.

Estimates of the dynamic viscosity in the top part of the lower mantle vary widely [2,35–38], even though it is now clear that very low values of the order of $2\text{--}4 \times 10^{21} \text{ Pa s}$ (e.g. [39,40]) are not required to explain postglacial uplift [41]. Observed plate motions and geoid modeling impose a viscosity contrast of about two orders of magnitude between upper and lower mantle [35,42,43]; it is the contrast that is best resolved, so that a proper evaluation of lower mantle viscosity depends on the upper mantle η . The viscosity in the upper mantle is dominated by (relatively weak) olivine. Both oceanic and continental observations indicate that below the asthenosphere η is

likely of the order of 10^{21} Pa s . Pressure will increase the viscosity under the oceans by a factor of about 1000 before diffusion creep kicks in [44], thus increasing η from 10^{18} Pa s [45] to 10^{21} Pa s . Behn et al. [46] find $3 \times 10^{19} \text{ Pa s}$ for the asthenospheric viscosity in the oceans surrounding Africa. Continental viscosity, as deduced from postglacial uplift, is already higher ($10^{20}\text{--}10^{21} \text{ Pa s}$) but its increase with depth is partially offset by the steeper geotherm. Given an upper mantle with 10^{21} Pa s , an increase by two orders of magnitude indicates a lower mantle viscosity of the order of 10^{23} Pa s . Lithgow–Bertelloni [35] finds a preferred average value of $5 \times 10^{22} \text{ Pa s}$. If the heat output of the Earth is used as a constraint, a lower bound of $3 \times 10^{22} \text{ Pa s}$ is found [47]. This is somewhat higher than the value obtained in a comprehensive study by Forte and Mitrovica [36] for a constant viscosity lower mantle, though they obtain excursions as high as 10^{24} Pa s at deeper levels when inverting for a depth-dependent viscosity model.

Rather than deal with a different value for the dynamic viscosity at every depth where we analyse the plume flux, we prefer to use η at 800 km as the standard for comparisons. Thus, η was fixed at a depth of 800 km, then extrapolated to other depths and temperatures using:

$$\eta(T) = \eta_R \exp(\beta T_m/T) \quad (8)$$

where β is the same parameter as defined in Eq. (6). The (undisturbed) temperature T increases from 1950 K at 800 km to 2425 K at 2000 km depth, the solidus temperature T_m rises in this interval from 3750 K to 4810 K. The constant η_R is determined from the η_{800} at 800 km depth. We adopt $\eta_{800} = 6 \times 10^{22} \text{ Pa s}$, which is at the high end of the range of published values. Changes in η_{800} have a simple effect on the flux estimates, since they multiply the viscosity by a constant factor overall. Since the term $\eta \nabla^2 v_z$ in Eq. (2) does not change if v_z is divided by the same constant, lowering η_{800} by a factor of 2 (to $3 \times 10^{22} \text{ Pa s}$) will simply double the flux estimates.

The uncertainty in η_{800} greatly exceeds the uncertainty in the other parameters. Assuming η_{800} is uncertain by a factor of three, this means practically that the flux calculations at 800 km are also uncertain by that factor. Extrapolation to larger depths easily increases the effective uncertainty in the viscosity- and hence in the flux- to a factor of 10. It is clear, though, that we cannot lower the viscosity by a factor of 10 from the values used here without being penalized with unacceptably high heat flux. There is, however, one factor that needs to be considered: chemical heterogeneity, in particular enrichment with volatiles or iron. Both influence the flux estimates, but in very different ways.

6. Chemical heterogeneity

It has been suggested that the lowermost mantle is enriched in iron [36,48–51]. The prime role of iron would be to make the plumes heavier and so reduce their buoyancy; a secondary (but much less important) effect is that iron reduces V_B , thus explaining away some of ΔV_P and thus reducing the temperature anomaly estimates. If the whole of the lower mantle is enriched in iron [52], only the temperature effect would operate, but of course the plumes would have reduced buoyancy upon entering the upper mantle. To be able to study both effects, we parameterize the plume enrichment by the ratio of abundances $X_{Fe} \equiv [Fe]/([Mg]+[Fe])$. This defines the density increase $\Delta\rho_{Fe}$, using $\partial \ln \rho / \partial X_{Fe} = 0.305$, neglecting the small effect on the molar volumes of MgO and perovskite [53]). We assume $\partial \ln V_p / \partial X_{Fe} = -0.17$ [54,55]. We studied enrichments of up to $\Delta X_{Fe} = 0.01$, keeping it constant over the entire plume cross-section.

Very high iron concentrations are not likely, as these will narrow down the plumes at the edges where the thermal buoyancy is not sufficient to overcome the negative chemical buoyancy, making them thinner than actually observed. For example, Fig. 10 shows the effect of iron enrichment computed for the tomographic modeling of the Tahiti plume at 1600 km depth. It shows the decrease in interpreted maximum temperature, which changes because part of the velocity anomaly is now attributed to the increase in iron, as well as the plume heat flux. The latter reduces quickly with increasing iron, because the buoyancy is reduced to zero or becomes even negative at the edge of the plume, thus restricting the radius of the conduit drastically. But this also restricts our ability to enrich the plumes with iron: even a modest iron enrichment of, $\Delta X_{Fe} = 0.005$ or 0.5% narrows the plumes too much—in the case of Tahiti from 1000 to 650 km at a depth of 1600 km—contradicting the tomographic evidence (see Fig. 5). An

enrichment of 0.003, halving the flux, is still acceptable in view of the lack of tomographic resolution. Higher plume enrichments may be possible if the iron is concentrated near the center of the plume, as it would be if entrained from a thin layer at the bottom of the lower mantle.

An excess of volatiles such as water influences the flux estimates potentially through its possibly strong effect on the attenuation (Q_P^{-1}), which plays a role in Eq. (5). No experimental studies are available, and quantifying its effect is difficult, especially if we consider that water may influence grain size and actually increase Q_P [37]. Fig. 10 indicates that the effect of volatiles is less than that of iron unless its effect on attenuation is very dramatic.

7. Discussion

It would be very valuable if we had high quality estimates of the mid-mantle heat flux Q_c as a function of viscosity, as well as of the buoyancy flux B , for all of the major plumes, since it would potentially provide a constraint on the viscosity—assuming all of the lower mantle flux eventually ends up at the surface. Where well resolved at mid-mantle depth (the filled circles in Fig. 9), tomographic flux estimates vary by a factor of about two over a depth range. This variation is probably not significant in view of the uncertainty in the temperature anomalies. We selected the depth below 1100 km that gave the least bias in the resolution tests as representative for the mid-mantle plume flux. As it turns out, for the major plumes that we can resolve, buoyancy flux estimates are only available for Azores, Canary/Cape Verde, Easter, the Hawaii plume (which splits up into two branches at mid-mantle depth), and Tahiti.

In Fig. 11 we compare these five flux estimates with published values taken from Table 11.2 in [56] (but originally from [4]). Even a cursory comparison of B and

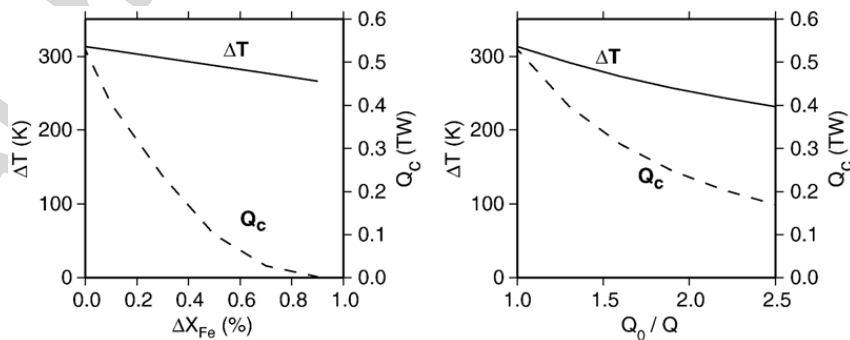


Fig. 10. The influence of plume iron (left) and volatiles (right) on the maximum plume temperature anomaly ΔT and the heat flux Q_c for the Tahiti plume at a depth of 1600 km, uncorrected for bias. ΔX_{Fe} is in percent, the influence of volatiles is parameterized by its influence on the attenuation ratio Q_0/Q , where Q is the quality factor of the enriched material, vs. Q_0 in the background model.

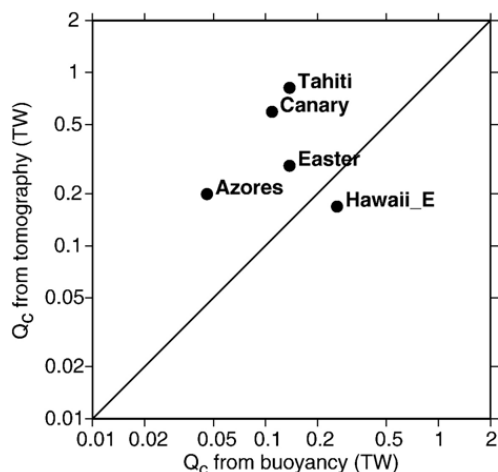


Fig. 11. Comparison of the heat fluxes estimated from tomography (selecting the depth with the smallest bias as determined by the resolution test) with Q_c derived from buoyancy flux observations at the surface [4]. ‘Canary’ combines the fluxes of Cape Verde and Canary. See discussion in text.

Q_c for these fluxes puts the validity of the use of B to estimate the full mantle flux in doubt. With the exception of Hawaii which has a flux slightly below the buoyancy estimate –but where the calculated flux does not include the unresolved contribution from the western branch– the other four plumes have heat flux estimates from the tomography that exceed those estimated from buoyancy ranging from a factor of about 2 for Easter to 6 for Tahiti. The latter may be too high if, as discussed before, Tahiti also feeds MacDonal and Marquesas. It is significant that our choice of viscosity is probably close to the highest acceptable value, because this implies that we cannot lower the tomographic flux by raising η . Fig. 11 strongly suggests that not all mantle flux is measurably visible in topographic swells. If we lower η_{800} to 1.5×10^{22} Pa s [36], the tomography flux estimates multiply by 4 and the differences become even more striking — even the eastern branch alone will have a flux larger than that estimated from Hawaii’s buoyancy flux. The strong linear dependence of flux on viscosity is different from the familiar scaling law for parameterized convection $Nu = Ra^{1/3}$. The reason is that in our analysis the plume geometry is –for the first time– constrained by (tomographic) observations, so that a change in η cannot change the geometry of the heat flux, only its value.

Note also that a number of plumes for which we have flux estimates in the lower mantle, have no known estimates from buoyancy observed at the surface for lack of a clearly identifiable swell, another indication that the total buoyancy flux underestimates the true total plume flux. Despite the uncertainties, it is safe to say that the true heat flux carried by the plumes is at least a factor of three,

and possibly (depending on viscosity) a factor of ten higher than the classic estimate of 3.3 TW — in other words, the tomography argues for a plume heat flux in the range of 10–30 TW. The strongest plumes have rise velocities of the order of a few cm/yr, and heat fluxes of the order of 1 W/m^2 , comparable to the very highest heat fluxes observed at the surface. Except for the heat flux, these characteristics are mostly in line with geodynamical expectations. In mid-mantle, the temperature anomaly at the center of the plumes is of the order of 300 K or more for the strongest plumes, but has decreased to about 200 K near the 670 discontinuity. In fact, if the 300 K anomaly were to survive to the surface it would lead to severe incompatibilities with the observed characteristics of basalts. For example the volume of Hawaiian basalts is only $0.2 \text{ km}^3/\text{yr}$ [57], and they do not show any komatiitic characteristics common to higher temperatures [58].

The large radius –and consequently high heat flux– is the major discrepancy between the tomographic observations and predictions from numerical modeling. For example, Zhong [24,59] predicts plume spacings, plume temperature gradients and rise velocities consistent with inferences from tomography, but a lower flux because of a much smaller predicted plume radius of the order of only 100 km. It is not possible to dismiss this discrepancy by arguing that the large radii observed in tomography are an artifact due to lack of resolution, because extensive resolution tests [15] have shown that plumes with a radius of only 100 km would simply not show up in tomographic images, even with use of finite-frequency theory. Furthermore, to generate the observed seismic delays, the temperature anomalies of thin plumes would have to be proportionally magnified and become incompatible with petrological inferences from hotspot basalts [58].

Not all numerical experiments predict thin plumes. An early study by Thompson and Tackley [60] found that for plumes governed by a temperature-dependent rheology (with an activation energy of 250 kJ/mol), a plume head develops with a radius of 500 km, which is reduced to 250 km for the conduit. This plume rises to the 670 km discontinuity in 92 My, equivalent to an average rise velocity of 2.4 cm/yr. A temperature anomaly of 500 K was maintained throughout the lower mantle, which reduced to 250 K upon arrival at the surface. The authors did not report the heat flux carried by this plume model but our estimate from the temperatures in their plots gives about 0.8 TW for one plume alone, which is much more compatible to the flux values inferred in this paper. And in a more recent numerical study, Goes et al. [61] conclude that plumes with a buoyancy flux below 4 Mg/s have difficulty surviving. Of the buoyancy fluxes listed by Sleep [4], only that of Hawaii satisfies this condition.

These results indicate that the discrepancy may be resolved by a more extensive exploration of the model parameter space by geodynamicists, and that a mid-mantle plume flux between 10 and 30 TW is not unphysical.

Does this leave room for other upward fluxes through the 670 that contribute to the heat flux? Davies [3] argues that the fluxes associated with slabs and plumes are independent, that each carries its own return flow. Apart from the fact that such a return flow of ‘normal’ mantle leads to a degree of mixing that makes it more difficult to explain the geochemical heterogeneities, such flow is not driven by significant temperature anomalies and thus of little or no influence to the heat budget. Small, undetectable plumes have been suggested to contribute significantly to the flux [62], but the physical reality of such a model has been questioned because the spacing of such plumes would be very much smaller than dictated by scaling laws [24]. Even if small plumes do exist, they may not have enough extra buoyancy to surmount resistance at the 670 discontinuity if the Clapeyron slope is negative. This is supported by our observed widening of many plumes below 670 km, and by the numerical studies of Goes et al. [61]. To penetrate the barrier, an extra force from high density material above (for slabs) or light material below (for plumes) is needed to provide the extra force. This makes it likely that *no material is exchanged between upper and lower mantle except in the form of plumes and slabs*.

Using reasonable estimates for different contributions [63] we estimate the contribution of the plumes to the total heat flux at 670 km depth. If one subtracts the contributions from radiogenic heat generation in the continental crust (less than 8 TW) and upper mantle (2 TW) and the upper mantle secular cooling (3 TW) from the total heat flux of the Earth (44 TW), about 31 TW has to cross the 670 km discontinuity. Davies [3] estimates that the total heat flux through the 670 km discontinuity amounts to 27 TW. This would have to be raised to 30 TW if the total heat flux of the Earth is 44 TW rather than the 41 TW assumed by Davies.

Much of the heat flux from lower- to upper mantle is actually accomplished by downward advection of cold slabs [23,64], but a precise estimate is difficult to give since not all subducted slab material penetrates the 670. Anderson [65] has a low estimate for the flux of all slabs, revised upwards to 12.7 TW in a note added to his paper. Using a more sophisticated model [66,67] and plate tectonic parameters from Bird [68], we obtain 14.4 TW. Both are lower than Davies’ 21 TW [3]. Thus, if the highest number is correct and all slabs end up in the lower mantle, a minimum of 6 TW is advected in the

upward direction. This number is almost certainly too small by a factor of two or more, and 12–18 TW is more realistic. Even if it would be as high as 20 TW, it is clear that this overlaps with the 10–30 TW flux from plumes as derived from seismic tomography. This analysis shows that –within the wide uncertainties– we cannot rule out that all of the upwards heat transport through the 670 km discontinuity is carried by plumes, and that the role of plumes is far more important than hitherto assumed.

It remains to address the cause of the discrepancy between B and mid-mantle Q_c . It is very well possible that the buoyancy flux at the surface as measured by the size of the topographic swell underestimates the heat flux at large depth, and that statements relating the surface buoyancy flux directly to the role of deep heat transport by mantle plumes are unjustified. In extrapolating surface flux to larger depth, several factors must be taken into account: the adiabatic cooling of the plume differs from that of the surrounding mantle, which may very well be sub-adiabatic because of internal heating [69]. A plume that does cool adiabatically as it rises will then see its temperature anomaly decrease. For slowly rising plumes, heat diffusion will gradually diminish the temperature within the conduit [59,70]. Heat loss from plumes was also shown to be important in the experimental study of Couilliette and Loper [71]. In a numerical study of convection, Bunge [72] finds that the surface buoyancy flux underestimates the deep flux by a factor of three. Zhong [59] finds a similar decrease but attributes part of it to diffusive, in addition to adiabatic, cooling.

However, a subadiabatic mantle is not likely to explain away all of the discrepancy –if only because this would leave the Earth’s heat budget short of many terawatts of heat flux. The remaining thermal anomaly is likely to reach the surface in one form or another. We have already mentioned the possibility that the Tahiti plume feeds both MacDonal and Marquesas, and that plume spreading below 670 km and spawning upper mantle plumes as proposed by Allègre [18] is a realistic possibility. Enrichment in iron, either of the lower mantle as a whole, or entrainment in the plumes, would promote ponding of plumes below 670, as we observed for several plumes.

A third factor to explain the discrepancy is spreading of a plume over a wide area by mixing of plume material with that of the low-viscosity asthenosphere. This process is perhaps more questionable but, as in the case of deeper spreading, has the potential to severely discredit fluxes estimated from short-wavelength topographic swells. In the study by Thompson and Tackley [60], the temperature

drop in the plume is much stronger in the upper mantle than in the lower mantle, which would not be expected for adiabatic or diffusive cooling, and we see this as a sign that deflection of plume material and mixing into the low-viscosity asthenosphere may be a process of importance. This idea, originally due to Morgan [73,44], was recently invoked by Romanowicz and Gung [11] to explain the strong pattern of shear wave anisotropy beneath the Pacific ocean. Behn et al. [46] find that asthenospheric flow driven by lower mantle upwelling best fits the observed anisotropy above the African Superplume. For Reunion, a channeling of material between plume and ridge has been observed directly [74]. Asthenospheric flow could also explain islands devoid of a lower mantle plume, like Bermuda.

Our findings have important implications for geodynamics. Our calculations suggest that the lower mantle viscosity is high, simply because values much lower than those in Fig. 6 could easily lead to a plume heat flux that exceeds the amount allowed by the Earth's heat budget.

At the very least, our research points to a new way of estimating plume heat flux based on observations, taking away part of the uncertainty associated with purely numerical modeling. We wish, however, also to make a case for a much larger role of plumes in the Earth's heat budget than hitherto assumed, despite the large uncertainties that our estimates still have. The physical model has strong simplifications, but is so far the only way to give a quantitative interpretation to the tomographic plume images and should at least provide an 'order of magnitude' flux estimate. It is significant that this estimate itself is an order of magnitude higher than earlier estimates based on buoyancy flux, despite using the highest acceptable viscosity in the lower mantle. Iron enrichment at the center of the plume could still lower the flux estimate and bring it in line with buoyancy flux, but the observations of plumes and slabs stalling at 670 km depth make it difficult to imagine what other transporters of heat can bring 31 TW across this boundary if the extra buoyancy of an extended flow such as associated with slabs and plumes is not provided for.

Acknowledgements

Uli Hansen kindly checked the accuracy of Eq. (2) against his numerical plume calculations. Shijie Zhong gave a very constructive review that significantly improved the original manuscript. GN acknowledges the hospitality of the Laboratoire de Géophysique Interne et Tectonophysique in Grenoble and the interactions with many colleagues there. Discussions with Nick Arndt, Tony Dahlen, David Stevenson and Albert Tarantola were very helpful. This research was supported by the NSF.

References

- [1] S. Franck, Evolution of the global mean heat flow over 4.6 Gyr, *Tectonophysics* 291 (1998) 9–18.
- [2] J. Korenaga, Energetics of mantle convection and the fate of fossil heat, *Geophys. Res. Lett.* 30 (2003) doi:10.1029/2003GL016982.
- [3] G. Davies, Topography: a robust constraint on mantle fluxes, *Chem. Geol.* 145 (1998) 479–489.
- [4] N. Sleep, Hotspots and mantle plumes: some phenomenology, *J. Geophys. Res.* 95 (1990) 6715–6736.
- [5] G. Davies, Ocean bathymetry and mantle convection 1, large-scale flows and hotspots, *J. Geophys. Res.* 93 (1988) 10467–10480.
- [6] R. Hill, I. Campbell, G. Davies, R. Griffiths, Mantle plumes and continental tectonics, *Science* 256 (1992) 186–193.
- [7] H.-C. Nataf, Seismic imaging of mantle plumes, *Annu. Rev. Earth Planet. Sci.* 28 (2000) 391–417.
- [8] B. Romanowicz, Global mantle tomography: progress status in the past 10 years, *Annu. Rev. Earth Planet. Sci.* 31 (2003) 303–328.
- [9] H. Bijwaard, W. Spakman, Tomographic evidence for a narrow whole mantle plume below Iceland, *Earth Planet. Sci. Lett.* 166 (1999) 121–126.
- [10] S. Goes, W. Spakman, H. Bijwaard, A lower mantle source for central European volcanism, *Science* 286 (1999) 1928–1931.
- [11] B. Romanowicz, Y. Gung, Superplumes from the core–mantle boundary to the lithosphere: implications for heat flux, *Science* 296 (2002) 513–516.
- [12] M. Rhodes, J. Davies, Tomographic imaging of multiple mantle plumes in the uppermost lower mantle, *Geophys. J. Int.* 147 (2001) 88–92.
- [13] D. Zhao, Seismic structure of hotspots and mantle plumes, *Earth Planet. Sci. Lett.* 192 (2001) 251–265.
- [14] F. Dahlen, S.-H. Hung, G. Nolet, Fréchet kernels for finite-frequency traveltimes — I. theory, *Geophys. J. Int.* 141 (2000) 157–174.
- [15] R. Montelli, G. Nolet, F. Dahlen, G. Masters, E. Engdahl, S.-H. Hung, Finite frequency tomography reveals a variety of plumes in the mantle, *Science* 303 (2004) 338–343.
- [16] R. Montelli, G. Nolet, F. Dahlen, G. Masters, A catalogue of deep mantle plumes: new results from finite-frequency tomography, *Geochem. Geophys. Geosys.* (G3) submitted for publication.
- [17] Y. Fukao, S. Widiyantoro, M. Obayashi, Stagnant slabs in the upper and lower mantle transition region, *Rev. Geophys.* 39 (2001) 291–323.
- [18] C. Allègre, Isotope geodynamics, *Earth Planet. Sci. Lett.* 86 (1987) 175–203.
- [19] L. Cserepes, D. Yuen, On the possibility of a second kind of mantle plume, *Earth Planet. Sci. Lett.* 183 (61–71) (2000).
- [20] M. Monnereau, D. Yen, Link between lower mantle superplume and upper mantle plume cluster, Abstracts, Superplume Workshop Tokyo, 2002.
- [21] K. Sigloch, G. Nolet, Measuring finite-frequency body wave amplitudes and travel times, *Geophys. J. Int.* (in press).
- [22] D. Loper, F. Stacey, The dynamical and thermal structure of deep mantle plumes, *Phys. Earth Planet. Inter.* 33 (1983) 304–317.
- [23] S. Labrosse, Hotspots, mantle plumes and core heat loss, *Earth Planet. Sci. Lett.* 99 (2002) 147–156.
- [24] S. Zhong, Dynamics of thermal plumes in three-dimensional isoviscous thermal convection, *Geophys. J. Int.* 152 (2005) 289–300.
- [25] N. Sleep, Thermal haloes around plume tails, *Geophys. J. Int.* 156 (2004) 359–362.

- [26] G. Nolet, S. Karato, R. Montelli, Flux estimates from tomographic plume images yield evidence for chemical stratification in the mantle, *EOS Trans. AGU* 85 (Fall 2004) Meet. Suppl.
- [27] B. Karki, S. R. Wentzovitch, S. de Gironcoli, First principles thermoelasticity of MgSiO₃-perovskite: consequences for the inferred properties of the lower mantle, *Geophys. Res. Lett.* 28 (2001) 2699–2702.
- [28] R. Wentzovitch, B. Karki, M. Cococcioni, S. de Gironcoli, Thermoelastic properties of MgSiO₃-perovskite: insights on the nature of the Earth's lower mantle, *Phys. Rev. Lett.* 92 (2004) 1–4 (018501).
- [29] S. Karato, Importance of anelasticity in the interpretation of seismic tomography, *Geophys. Res. Lett.* 20 (1993) 1623–1626.
- [30] B. Karki, R. Wentzovitch, S. de Gironcoli, S. Baroni, First principles determination of elastic anisotropy and wave velocities of MgO at lower mantle conditions, *Science* 286 (1999) 1705–1707.
- [31] Y. Aizawa, A. Yoneda, T. Katsura, E. Ito, T. Saito, I. Suzuki, Temperature derivatives of elastic moduli of MgSiO₃ perovskite, *Geophys. Res. Lett.* 31 (2004) L01602.
- [32] S. Karato, B. Karki, Origin of lateral variation of seismic wave velocities and density in the deep mantle, *J. Geophys. Res.* 106 (2001) 21771–21783.
- [33] A. Chopelas, Thermal expansivity of lower mantle phases MgO and MgSiO₃ perovskite at high pressure derived from vibrational spectroscopy, *Phys. Earth Planet. Inter.* 98 (1996) 3–15.
- [34] G. Fiquet, A. Dewaele, D. Andraut, M. Kunz, T.L. Bihan, Thermoelastic properties and crustal structure of MgSiO₃ perovskite at lower mantle pressure and temperature conditions, *Geophys. Res. Lett.* 27 (2000) 21–24.
- [35] C. Lithgow-Bertelloni, M. Richards, Cenozoic plate driving forces, *Geophys. Res. Lett.* 22 (1995) 1317–1320.
- [36] A. Forte, J. Mitrovica, Deep mantle high-viscosity flow and thermochemical structure inferred from seismic and geodynamic data, *Nature* 410 (2001) 1049–1056.
- [37] V. Solomatov, Grain size-dependent viscosity convection and the thermal evolution of the Earth, *Earth Planet. Sci. Lett.* 191 (2001) 203–212.
- [38] D. Yamazaki, S. Karato, Some mineral physics constraints on the rheology and the geothermal structure of Earth's lower mantle, *Am. Mineral.* 86 (2001) 385–391.
- [39] W. Peltier, A. Tushingham, Global sea level rise and the greenhouse effect: might they be connected, *Science* 244 (1989) 806–810.
- [40] J. Davis, J. Mitrovica, Glacial isostatic adjustment and the anomalous tide gauge record of eastern North America, *Nature* 379 (1996) 331–333.
- [41] J.X. Mitrovica, Haskell 1935 revisited, *J. Geophys. Res.* 101 (1996) 555–570.
- [42] B. Hager, M. Richards, Long-wavelength variations in Earth's geoid: physical models and dynamical implications, *Philos. Trans. R. Soc. Lond., A* 328 (1989) 309–327.
- [43] H. Bunge, M. Richards, J. Baumgardner, Mantle-circulation models with sequential data assimilation: inferring present-day mantle structure from plate-motion histories, *Philos. Trans. R. Soc. Lond., A* 360 (2002) 2445–2567.
- [44] J.P. Morgan, W. Morgan, Y.-S. Zhang, W. Smith, Observational hints for a plumefed, suboceanic asthenosphere and its role in mantle convection, *J. Geophys. Res.* 100 (1995) 12753–12767.
- [45] D. Wiens, S. Stein, Implications of oceanic intraplate seismicity for plate stresses, driving forces and rheology, *Tectonophysics* 116 (1985) 143–162.
- [46] M. Behn, C. Conrad, P. Silver, Detection of upper mantle flow associated with the African superplume, *Earth Planet. Sci. Lett.* 224 (2004) 259–274.
- [47] B. Hager, M. Richards, Long-wavelength variations in Earth's geoid: physical models and dynamical implications, *Philos. Trans. R. Soc. Lond., A* 328 (1989) 309–327.
- [48] R. van der Hilst, H. Kárason, Compositional heterogeneity in the bottom 1000 km of the Earth's mantle: toward a hybrid convection model, *Science* 283 (1999) 1885–1888.
- [49] S. Morse, A double magmatic heat pump at the core–mantle boundary, *Am. Mineral.* 85 (2000) 1589–1594.
- [50] L. Kellogg, B. Hager, R. van der Hilst, Compositional stratification of the deep mantle, *Science* 283 (1999) 1881–1884.
- [51] T. Nakagawa, P. Tackley, Effect of the thermo-chemical convection on the thermal evolution of the Earth's core, *Earth Planet. Sci. Lett.* 220 (2004) 107–119.
- [52] R. Jeanloz, E. Knittle, Density and composition of the lower mantle, *Philos. Trans. R. Soc. Lond., A* 328 (1989) 377–389.
- [53] D. Weidner, Y. Wang, Chemical- and clapeyron-induced buoyancy at the 660 km discontinuity, *J. Geophys. Res.* 103 (1998) 7431–7441.
- [54] L. Stixrude, R. Hemley, Y. Fei, H. Mao, Thermoelasticity of silicate perovskite and magesiowuestite and stratification of the Earth mantle, *Science* 257 (1992) 1099–1101.
- [55] B. Kiefer, L. Stixrude, R. Wentzovitch, Elasticity of (Mg, Fe)SiO₃-Perovskite at high pressures, *Geophys. Res. Lett.* 29 (2002) 1539.
- [56] G. Schubert, D. Turcotte, P. Olson, *Mantle convection in the earth and Planets*, CUP, Cambridge, 2001.
- [57] R. White, D. McKenzie, Mantle plumes and flood basalts, *J. Geophys. Res.* 100 (1995) 17543–17585.
- [58] N. Arndt, Komatiites, kimberlites, and boninites, *J. Geophys. Res.* 108 (2003) doi:10.1029/2002JB002157.
- [59] S. Zhong, Constraints on thermochemical convection of the mantle from plume heat flux, plume excess temperature, and upper mantle temperature, *J. Geophys. Res.* 111 (2006) doi:10.1029/2005JB003972.
- [60] P. Thompson, P. Tackley, Generation of mega-plumes from the core–mantle boundary in a compressible mantle with temperature-dependent viscosity, *Geophys. Res. Lett.* 25 (1998) 1999–2002.
- [61] S. Goes, F. Cammarano, U. Hansen, Synthetic seismic signature of thermal plumes, *Earth Planet. Sci. Lett.* 218 (2004) 403–419.
- [62] B. Malamud, D. Turcotte, How many plumes are there? *Earth Planet. Sci. Lett.* 174 (1999) 113–124.
- [63] P. van Keken, E. Hauri, C. Ballentine, Mantle mixing: the generation, preservation and destruction of chemical heterogeneity, *Annu. Rev. Earth Planet. Sci.* 30 (2002) 493–525.
- [64] E. Mittelstaedt, P. Tackley, Plume heat flow is much lower than cmb heat flow, *Earth Planet. Sci. Lett.* 241 (2006) 202–210.
- [65] O. Anderson, The power balance at the core–mantle boundary, *Phys. Earth Planet. Inter.* 131 (2002) 1–17.
- [66] M. Deal, G. Nolet, R. van der Hilst, Slab temperature and thickness from seismic tomography, 1. Method and application to Tonga, *J. Geophys. Res.* 104 (1999) 28789–28802.
- [67] M. Deal, G. Nolet, Slab temperature and thickness from seismic tomography 2. Izu Bonin, Japan and Kuril subduction zones, *J. Geophys. Res.* 104 (1999) 28803–28812.
- [68] P. Bird, An updated model of plate boundaries, *Geochem. Geophys. Geosyst.* 4 (2003) 1027.
- [69] R. Jeanloz, S. Morris, Is the mantle geotherm subadiabatic? *Geophys. Res. Lett.* 14 (1987) 335–338.
- [70] M. Albers, U. Christensen, The excess temperature of plumes rising from the core–mantle boundary, *Geophys. Res. Lett.* 23 (1996) 3567–3570.

- [71] D. Coulliette, D. Loper, Experimental, numerical and analytical models of mantle starting plumes, *Phys. Earth Planet. Inter.* 92 (1995) 143–167.
- [72] H.-P. Bunge, Low plumes excess temperature and high core heat flux inferred from non-adiabtic geotherms in internally heated mantle circulation models, *Phys. Earth Planet. Inter.* 153 (2005) 3–10.
- [73] W.J. Morgan, Convection plumes in the lower mantle, *Nature* 230 (1971) 42–43.
- [74] E. Debayle, J. L ev eque, Upper mantle heterogeneities in the Indian Ocean from waveform inversion, *Geophys. Res. Lett.* 24 (1997) 245–248.

Author's personal copy